ACS OMEGA

Open Access

http://pubs.acs.org/journal/acsodf

Article

Synthesis Method and Principle of Octahedral Hierarchical LTA Zeolite and Its Application to Enhance Catalytic Activity in Styrene Epoxidation

Junzhong Wang, Qiancheng Zhang,* Jie Bai,* and Michael North

Cite This: *ACS Omega* 2024, 9, 39673−39681

Read Online

ACCESS | Metrics & More | Article Recommendations | Supporting Information

ABSTRACT: A 4 Å zeolite prepared under the synergistic effect of intense ultrasound and a high-voltage electrostatic field had an octahedral structure rather than a conventional hexahedral structure. XPS and XRD analyses showed that the ratio of silicon to aluminum, 2θ peak position, and the corresponding crystal planes were the same as those in traditional hexahedral 4 Å zeolite, but some crystal planes were more prominent. SEM imaging showed that the octahedral zeolites had a larger particle size. Porosimetry (BET surface area and BJH analysis) showed that the octahedral zeolite had become a mesoporous zeolite, and its specific surface area increased and its pore size expanded, which was conducive to loading catalytically active materials and thus improving its catalytic performance. In this paper, the mechanism of formation of hierarchical LTA zeolite is discussed, and the octahedral hierarchical LTA zeolite is used to catalyze the epoxidation of styrene, giving very good results. It is concluded that the (600), (622), (642), and (644) crystal planes played a decisive role in the styrene epoxidation reaction, providing a realistic basis for explaining the crystal plane catalysis effect of the 4 Å zeolite. This new zeolite prepared under the synergistic effect of intense ultrasound and a high-voltage electrostatic field, being the first time to prepare the octahedral hierarchical LTA zeolite, is simple to produce, green, and environmentally friendly and has good economic development prospects compared to the use of templating agents, which not only provides ideas and simpler methods for optimizing the performance of traditional zeolites and developing new zeolites with better performance but also enhances the theoretical basis for preparing new zeolites.

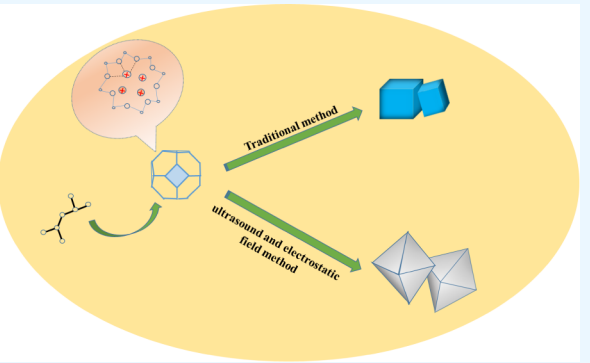

INTRODUCTION

The traditional 4 Å zeolite is a synthetic aluminosilicate with a microporous cubic lattice[1] and is one of the most used zeolites in the industry.[2] Because of its uniform pore structure, it is used as a solid adsorbent in sewage treatment and in the purification of environmental chemicals, water treatment, the metallurgical industry, soil improvement, and medicine through liquid or gas-phase separation processes.[1,2] In catalysis, although the uniform microporous structure of traditional 4 Å zeolite gives it the advantages of significant specific surface areas, outstanding thermal stability, and efficient shape selectivity, its narrow pores are not conducive to or even hinder the catalytic activity. The diffusion and transmission of medium and large molecular substances have caused problems such as low application efficiency associated with traditional microporous zeolites and serious catalytic deactivation.[3−5]

Mesoporous materials, due to their large specific surface areas, are conducive to the construction of plentiful surface active sites. Various means can be adopted to introduce catalytically active components and hence impart catalytic activity to a mesoporous material, such as guest loading in the mesopores, surface grafting, surface coating, and skeleton doping, forming a functionalized mesoporous catalytically active material or a functionalized mesoporous catalytic material.[6−8] Compared with microporous materials, mesoporous materials have higher specific surface areas and larger pore spaces, which enable the assembly of larger, more complex, and more varied catalytic sites, and have a smoother flow of reactants, intermediates, and products.[6−9] They can be applied in fields such as biological science and medicine, for protein immobilization and separation, in biochips, controlled drug release and treatment, mesoporous nanomedicine diagnosis and treatment, and targeted drug delivery.[8] Therefore, mesoporous materials have the potential to play an important role in the development of materials science in the future. However, the thermal stability, hydrothermal stability, and classic solid acid catalytic activity of classical silicate-based

Received: May 14, 2024
Revised: July 25, 2024
Accepted: July 31, 2024
Published: September 9, 2024

Scheme 1. Synthesis of Octahedral Hierarchical LTA Zeolites Through the Joint Application of Intense Ultrasound and a High-Voltage Electrostatic Field

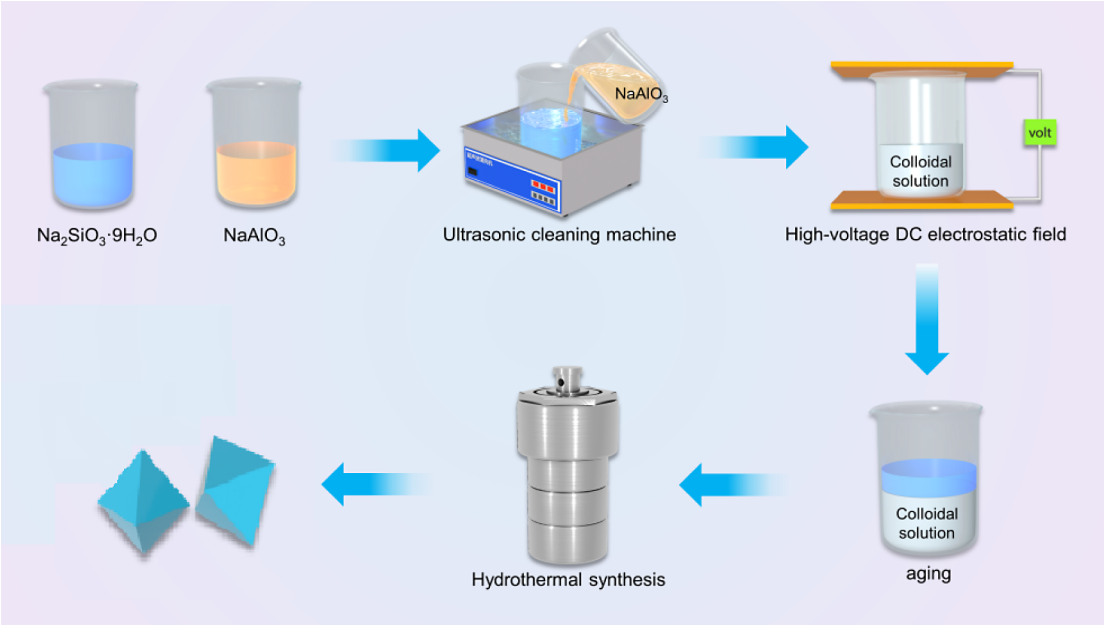

ordered mesoporous materials are still lower than those of conventional microporous zeolite crystals.[8,10]

In recent years, to improve the ion exchange performance and address the problems faced by zeolites, many scientists have devoted a lot of effort to overcome and remedy the weaknesses in this area.[11,12] Some of them have carried out pore expansion research and have made mesoporous, macroporous, and even microporous zeolites.[9,13,14] There are also many researchers who used technology and methods to selectively remove the amorphous structure in the material to prepare multilevel pores.[15−28,38] At present, using hard or soft templates to prepare multistage zeolites is very popular and has achieved very good results.[29−35] In our previous research, carbon nanofibers (CNFs) have been prepared by electrospinning and used as hard templates to synthesize hierarchical 4 Å zeolite.[36] In the above methods, external (typically organic) substances are used to expand the pores of zeolites instead of adjusting the structure of the zeolite itself and avoiding the use of other substances. This is inconsistent with the environmentally friendly, simple, and economical modern chemical concepts. In addition, there is still no research on the effect of different crystal planes within zeolite on catalytic reactions.

In the work reported herein, it was discovered that an octahedral zeolite that is different from the traditional hexahedral 4 Å zeolite was obtained by synthesizing the hierarchical LTA zeolite in the presence of ultrasound and an externally enhanced electrostatic field. XPS and XRD analyses of both the standard 4 Å zeolite and the hexahedral zeolite confirmed the change in structure. Porosimetry showed that the sample was a mesoporous zeolite. SEM imaging, XRD, porosimetry, and thermogravimetric analysis showed that the morphology of the octahedral zeolite had major changes compared to the traditional 4 Å zeolite. The relative prominence of some of its crystal planes increased in XRD patterns, the specific surface area increased, the pore diameter changed from microporous to mesoporous, and it had very good thermal stability. Furthermore, an octahedral zeolite was used to catalyze the styrene oxidation reaction, and the styrene conversion rate was greatly improved. It was found that the crystal planes of the zeolite that played a catalytic role in the styrene epoxidation process were enhanced, thus providing a realistic basis for explaining the enhanced catalysis of the hierarchical LTA zeolite.

EXPERIMENTAL SECTION

Materials. All reagents were sourced from Sinopharm Chemical Reagent Co., Ltd. and utilized as received without further purification.

Preparation. As the ratio of Si:Al:Na:H_2O was 1:1:3:75,[72] $Na_2SiO_3·9H_2O$ (10.65 g) was added to a beaker and dissolved in 20 mL of distilled water under magnetic stirring until a transparent solution was obtained. Separately, $NaAlO_3$ (3.85 g) was added to another beaker and dissolved in 17.5 mL of distilled water under magnetic stirring until a clear solution was formed. These two solutions were divided into two portions. One portion was processed to create hexahedral 4 Å zeolites following the literature method.[10] The other portion was transferred to a 50 Hz ultrasonic bath and the $NaAlO_3$ solution was added dropwise into the Na_2SiO_3 solution to form a colloidal solution with ultrasonic and mechanical stirring for 1 h (Scheme 1). The colloidal solution was then divided into five parts and placed in high-voltage DC vertical electrostatic fields with electric field strengths ranging from 10 to 23 kV (with 23 kV being the maximum due to the risk of sample discharge and field breakdown at higher voltages). The positive and negative copper plates were spaced 7 cm apart, with the liquid level 2 cm below the upper plate. After 1 h of treatment, the mixtures were aged for 24 h, followed by hydrothermal synthesis at 120 °C for 24 h. They were then cooled, washed with distilled water (2−3 times), suction-filtered, and dried at 120 °C to produce the novel zeolite samples.

Characterization. Characterization techniques included scanning electron microscopy (SEM) performed on a Phenom Pro machine (Netherlands) to examine the morphology and structure of the synthesized samples. Powder X-ray diffraction

https://doi.org/10.1021/acsomega.4c04461
ACS Omega 2024, 9, 39673−39681

(XRD) patterns were collected using a D/max 2500 PC (Rigaku, Japan) within a 2θ range of 5−80° to investigate the phase structure. A Simultaneous Thermal Analyzer (STA, Netzsch, STA449F3) was used for pyrolysis analysis. Inductively coupled plasma-optical emission spectrometry (ICP-OES) using an Agilent ICP-OES 725 ES (US) was performed to determine the elemental content. Pore size distribution and BET specific surface area were assessed via the Barrett−Joyner−Halenda (BJH) and Brunauer−Emmett−Teller (BET) methods, respectively. The degassing procedure involved pretreatment at 70 °C for 15 min, heating to 120 °C at 10 °C/min and holding for 15 min, then heating to 300 °C, and maintaining this temperature for 3 h.

Product analysis following styrene oxidation experiments was conducted using gas chromatography (GC) (Shimadzu 2010 Plus, RTX-5 capillary column, flame ionization detector) and GC−MS (Agilent 5975C). For the GC analysis, a temperature program of 10 °C/min was employed, starting from 60 up to 280 °C, with a final hold at 280 °C for 2 min. UV−vis absorption spectra were acquired by using a quartz cell on a Shimadzu UV-3150 spectrophotometer in Japan after diluting the solution with ethanol. To detect the presence of the 4 Å zeolite sample, we performed UV−vis diffuse reflection spectroscopy (UV−vis DRS, Shimadzu UV-3600). The elemental composition and valence states of the composite material were determined through X-ray photoelectron spectroscopy (XPS, Thermo Fisher Scientific ESCALAB 250).

Catalytic Performance. The following procedure was used to catalyze styrene epoxidation using zeolites: a test tube equipped with a magnetic stirrer and a condenser was loaded with 20 mg of zeolite, 1 mL of styrene, 5 mL of *tert*-butyl hydroperoxide as the oxidizing agent, and 5 mL of acetonitrile as the solvent (as illustrated in Scheme 2). The reactions

Scheme 2. Oxidation Reaction of Styrene Catalyzed by the Hierarchical LTA Zeolite

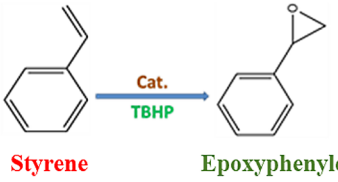

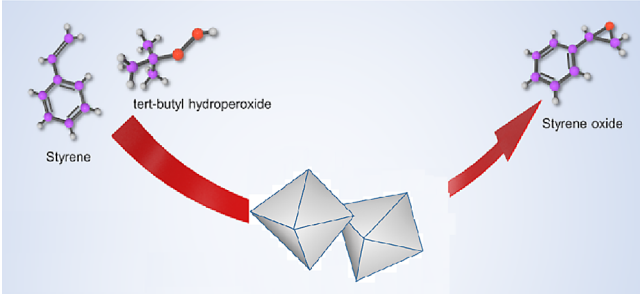

proceeded at 80 °C for 8 h under a nitrogen atmosphere. Following the reaction, the solid catalyst was isolated via centrifugation. The remaining solution was then transferred to an ethyl acetate/distilled water mixture in a beaker and stirred. After extraction and separation, the ethyl acetate layer's mixed solution was passed through a syringe filter prior to gas chromatography (GC) analysis. This experiment was conducted multiple times with various zeolites under identical conditions.

The transformation of styrene and the composition of each byproduct were deduced from the analysis of the gas chromatography (GC) peak zones. The calculation formulas for conversion and product selectivity were structured as follows: conversion of styrene (%) = (area of styrene converted) × 100/area of styrene before reaction; product selectivity (%) = (signal product area) × 100/area of all products (a calibration curve for each species has been plotted).

RESULTS AND DISCUSSION

Because cations that neutralize the negative charge of the aluminosilicate framework reside within the framework's pores and cavities[38−43] and are affected by the energy of the surrounding environment and their positions change, energy is instrumental in the fabrication and enhancement of zeolite properties.[10] In addition to the heating effect, other forms of energy such as microwaves[44] and electrostatic field[45] may also alter the spatial configuration of certain zeolites, potentially disrupting specific chemical bonds or activating them. Following numerous experiments and assessments, it was discovered that 4 Å zeolites changed from their conventional hexahedral to an octahedral form under specific ultrasonic and electrostatic field conditions with corresponding changes in both structure and performance.

SEM Analysis. Figure 1 shows SEM images of 4 Å zeolites prepared under different electrostatic field conditions. The

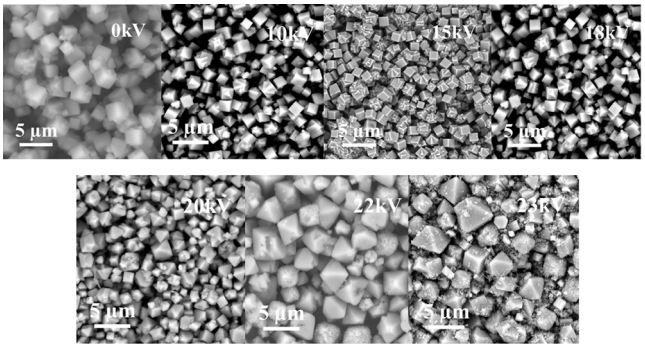

Figure 1. SEM images of the new zeolites in different electrostatic fields.

morphology of 4 Å zeolite is a regular hexahedron when the electric field voltage is 0 kV, and the average particle size is about 1.5 μm. However, if an electrostatic field were applied, the morphology of the 4 Å zeolites would be irregularly deformed. The degree of irregular deformation increased as the voltage of the applied electrostatic field increased, and the particle size also increased accordingly. When the applied electrostatic field voltage reached 20 kV, 4 Å zeolites began to appear with a regular octahedral morphology. As shown in Figure 1, the proportion of regular octahedral zeolites increased with the increase of the electrostatic field voltage. When the electrostatic field voltage reached the maximum (23 kV), the morphology of the zeolites was almost all regular octahedrons; the average particle size was about 4 μm, which reveals that the external electrostatic field exerted a profound influence on the zeolite's architecture; and the morphology has changed from the original hexahedron to a regular octahedron.

https://doi.org/10.1021/acsomega.4c04461
ACS Omega 2024, 9, 39673−39681

Once the zeolite attains an octahedral morphology, the particle size did not change further with an increase in the applied electrostatic field voltage.

X-Ray Diffraction (XRD) Analysis. XRD was used to analyze the solid-state structure of the sample. The zeolite powder XRD patterns were collected by using a D/max 2500 PC equipped with a Cu Kα line at 40 kV and 49 mA at a scanning rate of 10°/min with a step of 0.01°. Figure 2 shows

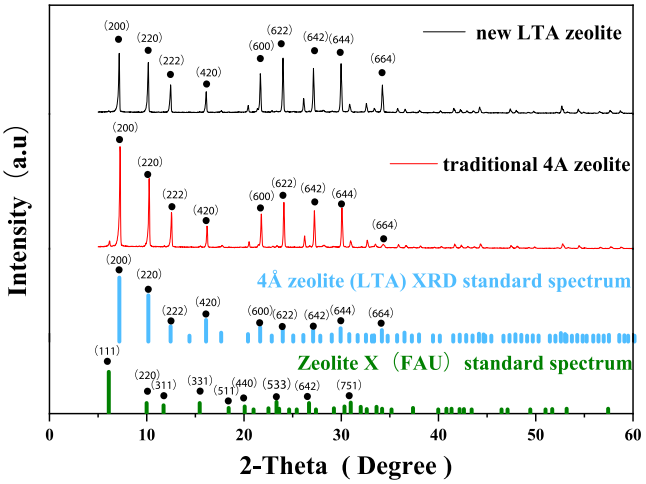

Figure 2. XRD patterns of hierarchical LTA zeolite, traditional 4 Å zeolite, and 4 Å zeolite (LTA), and zeolite X (FAU) XRD standard spectra.

the XRD patterns with clear reflections at 2θ of 7.2°, 10.2°, 12.4°, 16.1°, 21.6°, 24.0°, 27.1°, 29.9°, and 34.1°. Compared with 4 Å zeolite (LTA) and Zeolite X (FAU) XRD standard spectra, the peak positions completely matched only with 4 Å zeolite (LTA) (JCPDS no. 039-0222), indicating that the sample has the pure 4 Å zeolite structure instead of Zeolite X (FAU) (JCPDS no. 038-0237). The identified diffraction peaks are indicative of the lattice planes indexed as (200), (220), (222), (420), (600), (622), (642), (644), and (664), respectively. According to Figure 2, there is no other phase present in the octahedral samples prepared in a 23 kV electrostatic field, indicating that a pure 4 Å zeolite was synthesized. However, compared with the traditional 4 Å zeolite, which is a hexahedral 4 Å zeolite prepared according to the traditional method in relevant literature, the (600), (622), (642), and (644) crystal plane peaks of the hierarchical LTA zeolite have greater relative intensities. Figure 3 shows that the relative peak intensities of the (600), (622), (642), and (644) escalate with the increase of the electrostatic field intensity, indicating that these four crystal planes were increasingly exposed as the electrostatic field voltage increased.

BET and BJH Analysis. The N_2 adsorption−desorption isotherms of the new zeolites obtained under different electrostatic field conditions are shown in Figure 4. Based on the International Union of Pure and Applied Chemistry (IUPAC) classification, their nitrogen adsorption−desorption isotherms exhibit a uniform pattern of type I when the external electric field voltages are 0, 10, 15, and 18 kV, which is a method for estimating the pore structure of a material from gas adsorption measurements to provide an overview of void extent, indicating that they are microporous materials (seen in Figure 4A−D). When the electrostatic field intensities are 20, 22, or 23 kV, it can be seen that the isotherms are a

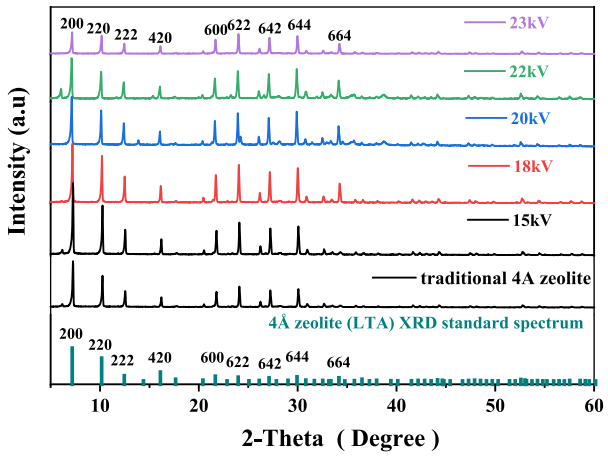

Figure 3. XRD patterns of hierarchical LTA zeolites and traditional 4 Å zeolites prepared in different electrostatic fields.

combination of type I and type IV (seen in Figure 4E−G). BET calculations showed that the specific surface areas of the samples with external electrostatic field voltages of 20, 22, and 23 kV are 423, 441, and 469 m^2 □g^{-1}, respectively, while the maximum specific surface area of the 4 Å zeolite prepared by traditional methods without any external field conditions (electric field voltage is 0 kV) is 258.26 m^2□g^{-1}. In the pore size distribution diagrams for these materials, it can be observed that the pore sizes around 4 nm appeared, showing that mesopores are generated under the electrostatic field voltage. It can be concluded that the new zeolite has changed from a microporous to a hierarchical material when the voltage exceeds 20 kV.

In Table 1, the surface area (BET) and micropore surface analyzed by the BJH test after different electric field intensities are shown. As seen in the table, if the electrostatic field voltage is less than 20 kV, the specific surface area is almost entirely micropores. If the electric field voltage is higher than or equal to 20 kV, the specific surface area of zeolite suddenly increases. Although micropores still account for the majority, their proportion has decreased significantly, and as the voltage increases, the proportion gradually decreases, which once again leads to the conclusion that the new zeolite has changed from a microporous to a hierarchical material when the voltage exceeds 20 kV.

XPS and ICP-OES Analyses. The main elements in the hierarchical LTA zeolite prepared in a 23 kV electrostatic field were determined by XPS characterization. Figure 5 shows that all expected chemical elements (C, Si, Al, O, and Na) are contained in the sample. The Si, Al, O, and Na are attributed to the zeolite sample while carbon comes from the uncovered conductive adhesive. The ratio of Si to Al (usually termed the "silicon-to-aluminum ratio") can be calculated from the total atom content of the XPS table to be about 1. To obtain the specific value of Si/Al, the mass fractions of Si and Al elements are obtained through ICP-OES test analysis, which showed that the Si content was 15.27 wt % and the Al content was 14.87 wt % after determined by ICP-OES, indicating that the silicon-to-aluminum ratio is about 1 as well.[37,46]

Catalyst Performance Test Results. The GC analysis outcomes for styrene epoxidation at 23 kV are illustrated in Figure S1. This figure indicates retention times of 2.523, 4.405, 5.410, 6.785, and 7.303 min corresponding to *tert*-butyl hydro peroxide, styrene, benzaldehyde, phenylacetaldehyde, and

https://doi.org/10.1021/acsomega.4c04461
ACS Omega 2024, 9, 39673−39681

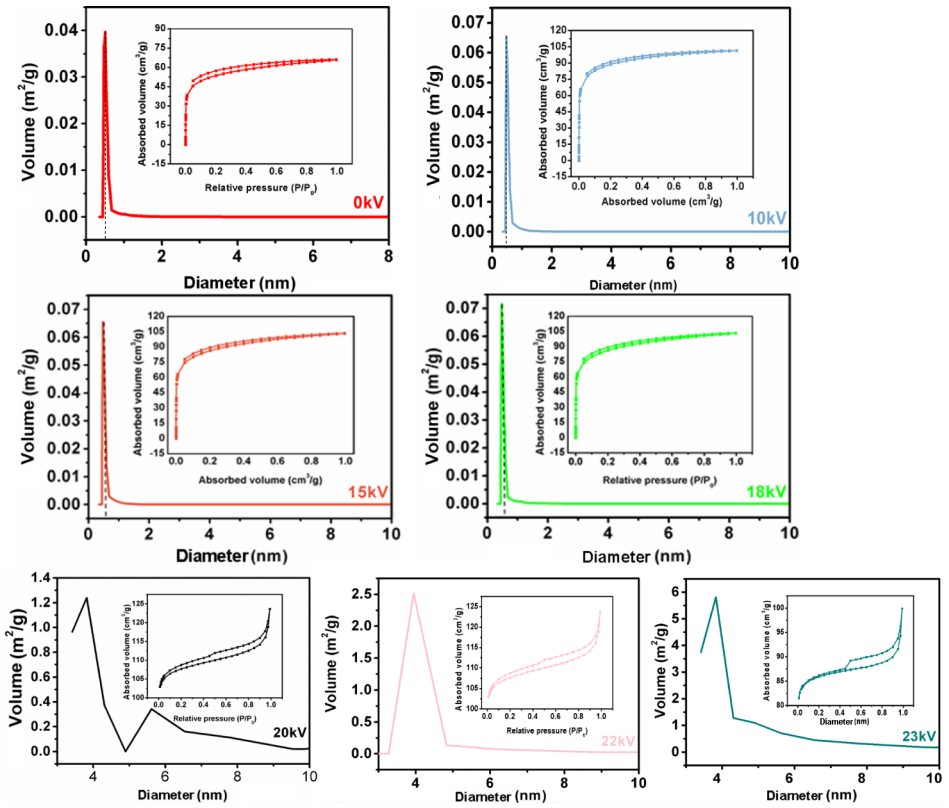

Figure 4. Pore size distributions and N_2 adsorption−desorption isotherms for the zeolites in different electrostatic fields.

Table 1. Surface Area (BET) and Micropore Surface Analyzed by the BJH Test After Different Electric Field Intensities

Electrostatic field voltage (kV)	0	10	15	18	20	21	23
Surface area (BET) (m^2/g)	258.261	263.377	277.504	290.736	423.138	441.220	469.126
Micropore surface (m^2/g)	258.254	263.332	277.423	290.618	407.212	420.145	423.187
Mesoporous surface (m^2/g)	0.007	0.045	0.081	0.118	15.926	21.075	45.939
Ratio of microporous surface/mesoporous surface	3.7×10^4	5.9×10^3	3.4×10^3	2.5×10^3	25.57	19.94	9.21

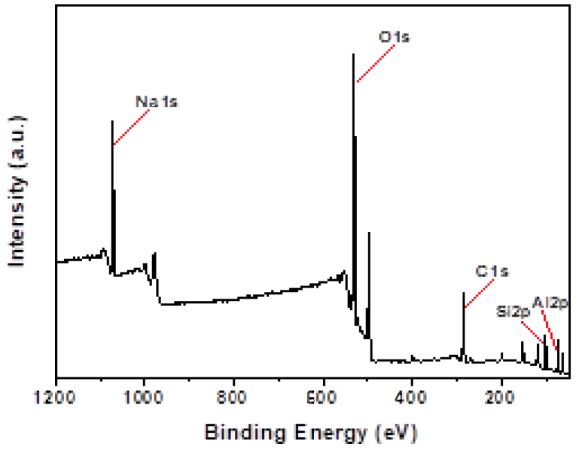

Figure 5. Full-scan XPS spectra of the octahedral hierarchical LTA zeolite in a 23 kV electrostatic field.

styrene oxide, respectively, closely matching the GC spectral data within the instrument database. It confirms the attainment of the targeted product. The zeolites prepared in 0, 10, 15, 18, 20, 22, and 23 kV electrostatic fields were used as catalysts for styrene epoxidation. The experimental results are shown in Table 2. When the zeolite was synthesized under an electric field intensity surpassing 20 kV, the styrene conversion escalated dramatically to a peak of 42%, markedly higher than the mere 8.3% conversion observed in the absence of a catalyst. This stark enhancement contrasts with the roughly 20% conversion rate achieved when the zeolite was generated using an external electrostatic field voltage of below 20 kV. The integration of BET and BJH analysis results alongside SEM imagery reveals that the octahedral hierarchical LTA zeolite boasts superior specific surface area and pore dimensions, facilitating superior access and reactivity for reactants as opposed to the hexahedral microporous zeolites. The cations

Table 2. Conversion of Styrene and Product Selectivity in Different Electrostatic Fields[a]

Electrostatic field voltage (kV)	0	10	15	18	20	22	23
Conversion (%)	19.6	20.3	20.7	21.2	33.4	36.2	42.3
Selectivity (%)	81.2	81.7	82.0	82.7	85.1	86.4	87.8

[a]Reaction conditions: catalyst (20 mg), styrene (1 mL), acetonitrile (5 mL), and TBHP (5 mL) at 80 °C for 8 h under a N_2 atmosphere.[72]

https://doi.org/10.1021/acsomega.4c04461
ACS Omega 2024, 9, 39673−39681

that originally formed the hexahedral zeolite to balance the aluminosilicate zeolite framework to carry charges and locate in the pores and cages of the zeolite move under the action of a strong electrostatic field and finally locate on the diagonal of the cubic unit cell, thus forming an octahedral zeolite. Due to the directional movement of ions, the atomic arrangement on the crystal plane leads to an increase in surface active sites, which can adsorb reactants and reduce the activation energy of the reaction to accelerate the reaction process. Simultaneously, these surface active sites allow the cationic backbone to activate the highly unstable perhydroxy anion ($\bullet OOH^-$) to form metal peroxo complexes, and the metal atoms attract styrene to form intermediates. Such active sites with specific geometries and chemical properties can guide reactant molecules to follow specific reaction pathways, thereby contributing to the production of specific product epoxides (styrene oxide).[10] In Figure 3, it can be seen that only (600), (622), (642), and (644) crystal planes change with the varying electric field strength when other conditions are not changed, which leads to the deformation of the zeolite, the increase of the pore size, and the exposure of more active sites, which can provide more reaction centers and improve catalytic efficiency. In addition, Table 1 shows that the conversion of styrene also gradually increases as the electrostatic field voltage increases, which is in line with the increase in relative strength of (600), (622), (642), and (644) crystal planes as the electrostatic field voltage increases, as shown in Figure 3. The increased prominence of these crystal planes suggests that these planes play a decisive role in the catalytic process. However, the conversion of styrene does not change much when the external electrostatic field voltage used to produce the zeolite is less than 20 kV, while it increases significantly when the external electrostatic field voltage is over 20 kV, which indicates that the octahedral hierarchical LTA zeolite is more conducive to exposing the four crystal planes, enhancing its catalytic activity and improving the rate of the reaction.

TG Analysis. After the catalyst performance test, the sample prepared under the 23 kV voltage condition with the best performance was taken for thermal stability testing. Figure 6 illustrates the thermogravimetric analysis conducted under nitrogen for the zeolite synthesized within a 23 kV electrostatic field. The analysis of the mass decrease curve indicates that the zeolite experiences a thermal mass reduction of 17.86% from 0 to 200 °C, attributed to the evaporation of water molecules adhered to its external surface. A further mass reduction of 3.82% between 200 and 480 °C is due to transformations occurring at the surface level. Beyond 480 °C, there is negligible mass loss. As depicted in Figure 7, following thermogravimetric analysis up to 800 °C, the crystal structure, BET surface area, and XRD pattern peaks remain largely unchanged. This demonstrates the exceptional high-temperature thermal stability of the zeolite, effectively addressing the typical issue of inadequate thermal stability found in mesoporous zeolites.

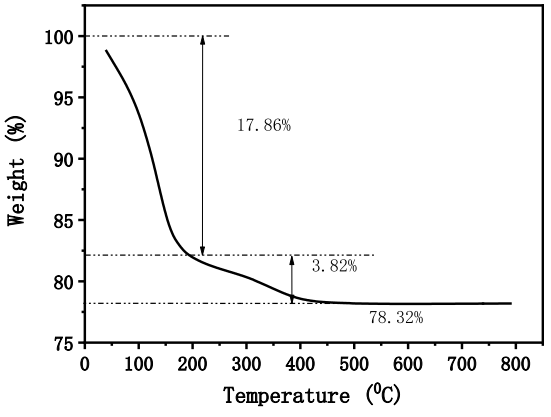

Figure 6. Thermogravimetric analysis of the octahedral hierarchical LTA zeolite prepared in a 23 kV electrostatic field.

Mechanism Analysis. The framework of aluminosilicate zeolite is composed of SiO_4 tetrahedra and AlO_4 tetrahedra.[37] The traditional 4 Å zeolite belongs to the LTA framework structure.[5,47,48,50−53] In this LTA framework structure, the SiO_4 and AlO_4 tetrahedra are meticulously organized, featuring a silicon-to-aluminum ratio that approximates one.[10,54] In this structure, the positive ions necessary to balance the aluminosilicate zeolite framework's negativity are situated within the zeolite's cavities and channels.[38−43,54,55] In the eight-membered ring structure of the LTA zeolite, every sodium ion (Na^+) has the proximity to interact with up to three framework oxygen atoms.[54] These ions exhibit random hopping behavior or remain stationary, occupying various positions within the ring while maintaining equivalence. This dynamic nature of the Na^+ ions contributes to the unique properties of the LTA zeolite's eight-membered ring.[10] Due to its exceptional insulating properties, characterized by little charge leakage and an absence of interface states, SiO_2 typically remains unaffected by external electric fields under ordinary conditions.[56−60] Nevertheless, as the SiO_2 layer's thickness approaches or falls below 1 nm, a significant enhancement in the electric field effect is observed.[56,58−60] In this study, the application of intense ultrasonic cavitation[61−63] resulted in more homogeneously sized particles and a notably reduced thickness of the colloidal SiO_2 to below 1 nm (as depicted in Figure 8), significantly impacting the system through the vertical electric field effect. Initially, the anions and cations within the conventional hexagonal 4 Å zeolite (such as the LTA) framework experienced strong polarization. Additionally, during the synthesis of the 4 Å zeolite, the colloidal nature of the entire system meant that the colloid itself was also influenced by the vertical electric field effect.[64,65] Moreover, given that the system was a colloidal aqueous solution, the colloid settled under gravity over time, creating a distinct boundary with the aqueous phase. When subjected to a powerful vertical electric field and gravitational forces, the surface tension of both the water and the colloid increased, as did the electric dipole moment. Throughout the aging process, water and colloids polarized by the vertical electric field maintained a significant electric dipole moment.[66,67] Consequently, during the initial stages of zeolite nucleation, when the electrostatic field voltage exceeded or equaled 20 kV, the negatively charged central oxygen atoms and nearby free Na^+ ions[49] on the existing framework were stretched, leading to the development of an octahedral shape (as illustrated in Scheme 3). Under the influence of a robust electric field, the material's form transitioned to an octahedron, which introduced additional mesoporosity without altering the fundamental crystal structure, as evidenced by the low-angle XRD patterns (Figure 9) and XRD patterns (Figure 2). This observation aligns closely with the findings reported by Wang et al.[73] and Liu et al.,[74] who noted that while the material's morphology changed, the crystal structure and the molecular sieve remained fundamentally unchanged. The disordered meso-

https://doi.org/10.1021/acsomega.4c04461
ACS Omega 2024, 9, 39673−39681

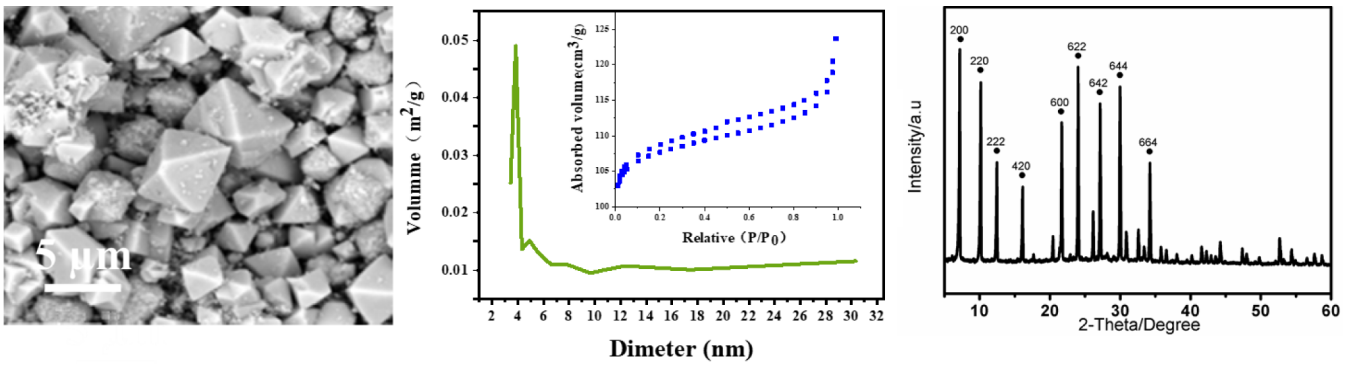

Figure 7. SEM and BET images and XRD pattern of the octahedral hierarchical LTA zeolite obtained in a 23 kV electrostatic field after thermogravimetric analysis.

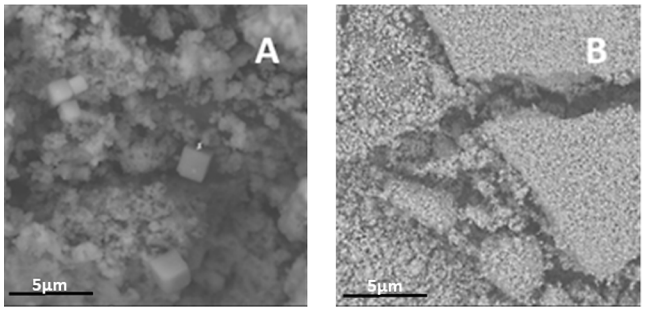

Figure 8. SEM images of colloidal particles and thickness of samples before (A) and after (B) ultrasonication.

Scheme 3. Formation of Octahedral Hierarchical LTA Zeolite

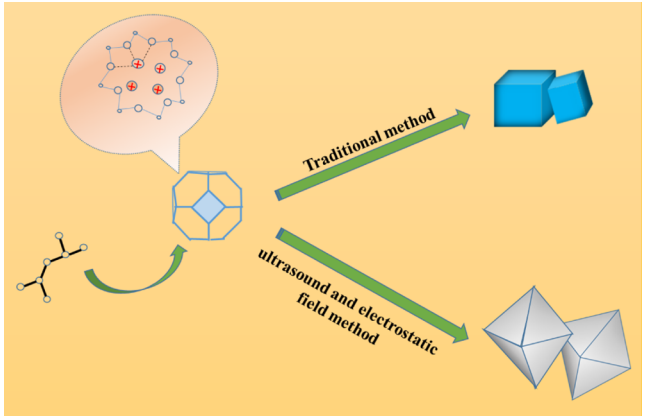

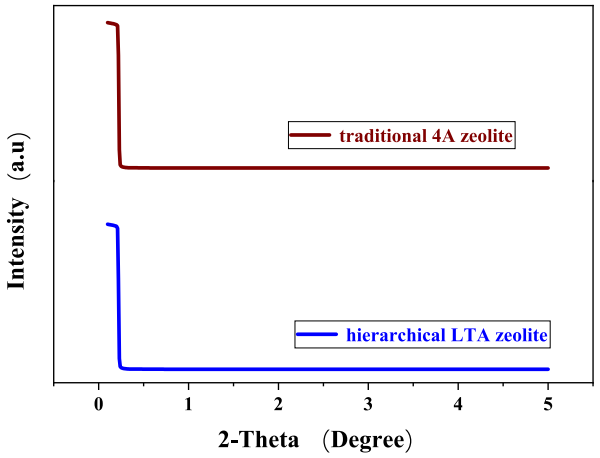

Figure 9. Low-angle XRD patterns of traditional 4 Å zeolites and hierarchical LTA zeolites.

pores do not produce clear diffraction peaks in the low-angle XRD patterns. However, the BET results clearly indicate an increase in the mesoporosity due to the ultrasonic electrostatic field. Following aging and hydrothermal synthesis, an octahedral zeolite framework was established. Due to the ABCABC stacking pattern of the octahedral hierarchical LTA zeolite (similar to FAU), the pore volume and pore channels expand,[68−71] explaining why the silicon-to-aluminum ratio and XRD diffraction peaks matched those of traditional 4 Å zeolites, while BET and BJH analyses revealed the creation of a mesoporous material with larger particle sizes observed in SEM images, thereby enhancing the catalyst's catalytic performance.

CONCLUSIONS

In summary, the zeolite prepared after the combined action of ultrasound and a high-voltage electrostatic field changed from a traditional hexahedral structure to an octahedral structure. Its specific surface area and pore size increased and the microporous zeolite became mesoporous. These features are more conducive to loading catalytically active materials and improving their catalytic performance. In addition, in the hierarchical LTA zeolite, four crystal planes were more exposed, and a crystal plane effect occurred in styrene oxidation, thereby greatly improving the catalytic performance. That the (600), (622), (642) and (644) crystal planes play a decisive role in this reaction provides a realistic basis for explaining the catalytic results. Moreover, this is the first time a new zeolite is prepared by the action of external physical factors, which is simple and has good development prospects in terms of environmental protection and economics, compared to the use of templating agents. It not only provides ideas and simpler methods for optimizing the performance of the original zeolite and developing new zeolites with better performance but also enriches the theoretical basis of the new zeolite preparation as well.

ASSOCIATED CONTENT

Supporting Information

The Supporting Information is available free of charge at https://pubs.acs.org/doi/10.1021/acsomega.4c04461.

https://doi.org/10.1021/acsomega.4c04461
ACS Omega 2024, 9, 39673−39681

GC analysis results for styrene epoxidation at 23 kV (PDF)

AUTHOR INFORMATION

Corresponding Authors

Qiancheng Zhang − *College of Chemical Engineering, Inner Mongolia University of Technology, Hohhot 010051, China*; Email: 982331943@qq.com

Jie Bai − *College of Chemical Engineering, Inner Mongolia University of Technology, Hohhot 010051, China*; orcid.org/0000-0002-7662-8238; Email: baijie@imut.edu.cn

Authors

Junzhong Wang − *College of Chemical Engineering, Inner Mongolia University of Technology, Hohhot 010051, China*; orcid.org/0009-0002-4353-1074

Michael North − *Green Chemistry Centre of Excellence, University of York, York YO10 5DD, U.K.*; orcid.org/0000-0002-6668-5503

Complete contact information is available at: https://pubs.acs.org/10.1021/acsomega.4c04461

Author Contributions

The manuscript was written through contributions of all authors. All authors have given approval to the final version of the manuscript.

Notes

The authors declare no competing financial interest.

ACKNOWLEDGMENTS

This work was supported by the Inner Mongolia National Science Foundation (2020LH02002)

REFERENCES

(1) Davis, M. E. Ordered porous materials for emerging applications. *Nature* **2002**, *417*, 813−821.

(2) Corma, A.; Diaz-Cabanas, M.; Martinez-Triguero, J.; Rey, F.; Rius, J. A large-cavity zeolite with wide pore windows and potential as an oil refining catalyst. *Nature* **2002**, *418*, 514−517.

(3) GuisnetM, G. J. P. *Zeolites for Cleaner Technologies*; ICP: London, 2002; pp. 261301.

(4) Wu, C. G.; Bein, T. Conducting Polyaniline Filaments in a Mesoporous Channel Host. *Science* **1994**, *264*, 1757−1759.

(5) Sahner, K.; Hagen, G.; Schoenauer, D.; Reiss, S.; Moos, R. Zeolites — Versatile materials for gas sensors. *Solid State Ionics* **2008**, *179* (40), 2416−2423.

(6) Yuhan, S.; Yan, M. Catalysis and function*Nanoporous material chemistry-catalysis and functionalization*; Yu, J.; Yan, W.; Science Press, Beijing, 2013, 125155.

(7) Qianjun, H.; Chen, Y.; Jianlin, S. Catalysis and function. In *Nanoporous material chemistry-catalysis and functionalization*; Yu, J.; Yan, W., Eds.; Science Press: Beijing, 2013.

(8) Estermann, M.; McCusker, L. B.; Baerlocher, C.; Merrouchet, A.; Kesslert, H. A synthetic gallophosphate molecular sieve with a 20-tetrahedral-atom pore opening. *Nature* **1991**, *352* (6333), 320−323.

(9) Corma, A. From microporous to mesoporous molecular sieve materials and their use in catalysis. *Chem. Rev.* **1997**, *97*, 2373−2419.

(10) Ruren, X.; Pang, W.; Jihong, Y.; Huo, Q.; Chen, J. *Chemistry of Zeolites and Related Porous Materials: Synthesis and Structure*; John Wiley & Sons, 2007. DOI: .

(11) Dongyuan, Z.; Ying, W.; Wuzong, Z. *Ordered mesoporous molecular sieve materials*; Higher Education Press: Beijing, 2013.

(12) Iwarnoto, M. Zeolites in Environmental Catalysis. *Stud. Surf. Sci. Catal.* **1994**, *84*, 1395−1410.

(13) Weitkamp, J. Zeolites and catalysis. *J. Solid State Ionics* **2000**, *131*, 175−188.

(14) Al-Jubouri, S. M.; Holmes, S. M. Hierarchically porous zeolite X composites for manganese ion-exchange and solidification: Equilibrium isotherms, kinetic and thermodynamic studies. *Chem. Eng. J.* **2017**, *308*, 476−491.

(15) Perez-Ramirez, J.; Christensen, C. H.; Egeblad, K.; Christensen, C. H.; Groen, J. C. Hierarchical zeolites: Enhanced utilisation of microporous crystals in catalysis by advances in materials design. *Chem. Soc. Rev.* **2008**, *37*, 2530−2542.

(16) Tao, Y. S.; Kanoh, H.; Abrams, L.; Kaneko, K. Mesopore-Modified Zeolites: Preparation, Characterization, and Applications. *Chem. Rev.* **2006**, *106*, 896−910.

(17) Egeblad, K.; Christensen, C. H.; Kustova, M.; Christensen, C. H. Templating mesoporous zeolites. *Chem. Mater.* **2008**, *20*, 946−960.

(18) Al-Jubouri, S. M.; Curry, N. A.; Holmes, S. M. Hierarchical porous structured zeolite composite for removal of ionic contaminants from waste streams and effective encapsulation of hazardous waste. *J. Hazard. Mater.* **2016**, *320*, 241−251.

(19) Xiao, J. J.; Li, H.; Zhu, G. B. Hierarchically porous MFI zeolite synthesized by zeolite seeding and alkaline steaming-mediated crystallization. *Adv. Powder Technol.* **2016**, *27*, 1396−1403.

(20) Verboekend, D.; Nuttens, N.; Locus, R.; Van Aelst, J.; Verolme, P.; Groen, J. C.; Perez-Ramirez, J.; Sels, B. F. Synthesis, characterisation, and catalytic evaluation of hierarchical faujasite zeolites: Milestones, challenges, and future directions. *Chem. Soc. Rev.* **2016**, *45*, 3331−3352.

(21) Zhang, Y. C.; Zhu, K. K.; Zhou, X. G.; Yuan, W. K. Hierarchically porous zeolite beta synthesized via steam-assisted crystallization of silanized dry gel. *Mater. Lett.* **2014**, *131*, 214−216.

(22) Li, H.; Jin, J. J.; Wu, W.; Chen, C. C.; Li, L.; Li, Y. S.; Zhao, W. R.; Gu, J. L.; Chen, G. R.; Shi, J. L. Synthesis of a hierarchically macro-/mesoporous zeolite based on a micro-emulsion mechanism. *J. Mater. Chem.* **2011**, *21*, 19395−19401.

(23) Verboekend, D.; Milina, M.; Pérez-Ramírez, J. Hierarchical Silicoaluminophosphates by Postsynthetic Modification: Influence of Topology, Composition, and Silicon Distribution. *Chem. Mater.* **2014**, *26*, 4552−4562.

(24) Janssen, A. H.; Koster, A. J.; De Jong, K. P. On the Shape of the Mesopores in Zeolite Y: A Three-Dimensional Transmission Electron Microscopy Study Combined with Texture Analysis. *J. Phys. Chem. B* **2002**, *106*, 11905−11909.

(25) Muller, M.; Harvey, G.; Prins, R. Comparison of the dealumination of zeolites beta, mordenite, ZSM-5 and ferrierite by thermal treatment, leaching with oxalic acid and treatment with $SiCl_4$ by ^{1}H, ^{29}Si and ^{27}Al MAS NMR. *Microporous Mesoporous Mater.* **2000**, *34*, 135−147.

(26) Van Aelst, J.; Haouas, M.; Gobechiya, E.; Houthoofd, K.; Philippaerts, A.; Sree, S. P.; Kirschhock, C. E. A.; Jacobs, P.; Martens, J. A.; Sels, B. F.; Taulelle, F. Hierarchization of usy zeolite by NH_4OH. a postsynthetic process investigated by NMR and XRD. *J. Phys. Chem. C* **2014**, *118*, 22573−22582.

(27) Van Aelst, J.; Verboekend, D.; Philippaerts, A.; Nuttens, N.; Kurttepeli, M.; Gobechiya, E.; Haouas, M.; Sree, S. P.; Denayer, J. F. M.; Martens, J. A.; Kirschhock, C.E.A.; Taulelle, F.; Bals, S.; Baron, G.V.; Jacobs, P.A; Sels, B.F. Catalyst design by nh$_4$oh treatment of usy zeolite. *Adv. Funct. Mater.* **2015**, *25*, 7130−7144.

(28) Yan, M.; Tian, X.; Peng, G.; Cao, Y.; Li, D. Hierarchically porous materials prepared by selective laser sintering. *Mater. Des.* **2017**, *135*, 62−68.

(29) Janssen, A. H.; Schmidt, I.; Jacobsen, C. J. H.; Koster, A. J.; de Jong, K. P. Exploratory study of mesopore templating with carbon during zeolite synthesis. *Microporous Mesoporous Mater.* **2003**, *65*, 59−75.

(30) Jacobsen, C. J. H.; Madsen, C.; Houzvicka, J.; Schmidt, I.; Carlsson, A. Mesoporous zeolite single crystals. *J. Am. Chem. Soc.* **2000**, *122*, 7116−7117.

(31) Zhu, K.; Egeblad, K.; Christensen, C. H. Mesoporous carbon prepared from carbohydrate as hard template for hierarchical zeolites. *Eur. J. Inorg. Chem.* **2007**, *2007*, 3917.
(32) Schmidt, I.; Krogh, A.; Wienberg, K.; Carlsson, A.; Brorson, M.; Jacobsen, C. J. H. Catalytic epoxidation of alkenes with hydrogen peroxide over first mesoporous titanium-containing zeolite. *Chem. Commun.* **2000**, *21*, 2157−2158.
(33) Kruk, M.; Jaroniec, M.; Ryoo, R.; Joo, S. H. Characterization of ordered mesoporous carbons synthesized using MCM-48 silicas as templates. *J. Phys. Chem. B* **2000**, *104*, 7960−7968.
(34) Shin, H. J.; Ryoo, R.; Kruk, M.; Jaroniec, M. Modification of SBA-15 pore connectivity by high-temperature calcination investigated by carbon inverse replication. *Chem. Commun.* **2001**, *4*, 349−350.
(35) Tong, Y. C.; Zhao, T. B.; Li, F. Y.; Wang, Y. Synthesis of monolithic zeolite beta with hierarchical porosity using carbon as a transitional template. *Chem. Mater.* **2006**, *18*, 4218−4220.
(36) Wu, Y. K.; Li, C. P.; Bai, J. Preparation of silver supported porous 4A-zeolite through hard template agent combined with heat treatment and study on its catalytic performance. *J. Porous Mater.* **2018**, *25*, 1669−1677.
(37) Takaishi, T. Ordered distribution of Na ions in dehydrated NaX zeolite. *Zeolites* **1996**, *17*, 389−392.
(38) Gramlich, V.; Meier, W. M. Crystal structure of hydrated NaA: A detailed refinement of a pseudosymmetric zeolite structure. *Z. Krystallogr.* **1971**, *133*, 134−149.
(39) Reed, T. B.; Breck, D. W. Crystalline zeolites. II. crystal structure of synthetic zeolite, type A. *J. Am. Chem. Soc.* **1956**, *78*, 5972−5977.
(40) Kerr, G. T. Chemistry of crystalline aluminosilicates. III. the synthesis and properties of zeolite ZK-5. *Inorg. Chem.* **1966**, *5*, 1539−1541.
(41) kühl, G. H. High-silica analogs of zeolite a containing intercalated phosphate. *Inorg. Chem.* **1971**, *10*, 2488−2495.
(42) Lok, B. M.; Messina, C. A.; Patton, R. L.; Gajek, R. T.; Cannan, T. R.; Flanigen, E. M. Silicoaluminophosphate zeolite: Another new class of microporous crystalline inorganic solids. *J. Am. Chem. Soc.* **1984**, *106*, 6092−6093.
(43) Simmen, A.; Patarin, J.; Baerlocher, C. *Proceedings of the 9th International Zeolite Conference*; Butterworth-Heinemann: Oxford, 1993. pp. 433440.
(44) Jain, A.; Soumik, D.; Barman, P. Microwave-assisted synthesis and notable applications of Schiff-base and metal complexes: A comparative study. *Res. Chem. Intermed.* **2022**, *48* (5), 2199−2251.
(45) Liu, Y.; Wang, Z.; Liu, C.-J. Mechanism of template removal for the synthesis of molecular sieves. *Catal. Today* **2015**, *256*, 137−141.
(46) Mannhart, J. High-Tc transistors. *Supercond. Sci. Technol.* **1996**, *9*, 49−67.
(47) Newman, A. C. D. A simple apparatus for separating fluorine from aluminosilicates by pyrohydrolysis. *Analyst* **1968**, *96*, 827−831.
(48) Newsam, J. M. The zeolite cage structure. *Science* **1986**, *231*, 1093−1099.
(49) van Bekkum H, H.; Flanigen, E. M.; Jacobs, P. A. *Zeolites and Zeolite: An Historical Perspective*; Elsevier Science B.V., 2001.
(50) Feuerstein, M.; Lobo, R. F. Characterization of Li cations in Zeolite LiX by solid-state NMR spectroscopy and neutron diffraction. *Chem. Mater.* **1998**, *10*, 2197−2204.
(51) Costenoble, M. L.; Mortier, W. J.; Uytterhoe, J. B. Location of cations in synthetic zeolites X and Y. Part 4.—Exchange limiting factors for Ca2+ in zeolite Y. *J. Chem. Soc., Faraday Trans. 1* **1976**, *72*, 1877−1883.
(52) Vitale, G.; Mellot, C. F.; Bull, L. M.; Cheetham, A. K. Neutron Diffraction and Computational Study of Zeolite NaX: Influence of SIII' Cations on Its Complex with Benzene. *J. Phys. Chem. B* **1997**, *101*, 4559−4564.
(53) Kim, Y.; Han, Y. W.; Seff, K. Crystal structure of fully dehydrated fully Tl^{+}-exchanged zeolite X. *Zeolites* **1997**, *18*, 325−333.
(54) Shibata, W.; Seff, K. Crystal Structure of a Sodium sorption complex of zeolite X containing linear Na_3^{2+} clusters. *J. Phys. Chem. B* **1997**, *101*, 9022−9026.
(55) Porcher, F.; Souhassou, M.; Dusausoy, Y.; Lecomte, C. The crystal structure of a low-silica dehydrated NaX zeolite. *Eur. J. Mineral.* **1999**, *11*, 333−343.
(56) Ahn, C. H.; Triscone, J. M.; Mannhart, J. Electric field effect in correlated oxide systems. *Nature* **2003**, *424*, 1015−1018.
(57) Arden, W. M. The International Technology Roadmap for Semiconductors—Perspectives and challenges for the next 15 years. *Curr. Opin. Solid St.* **2002**, *6* (5), 371−377.
(58) Hubbard, K. J.; Schlom, D. G. Thermodynamic stability of binary oxides in contact with silicon. *J. Mater. Res.* **1996**, *11*, 2757−2776.
(59) McKee, R. A.; Walker, F. J.; Chisholm, M. F. Crystalline oxides on silicon: The first five monolayers. *Phys. Rev. Lett.* **1998**, *81*, 3014−3017.
(60) Lin, A.; Hong, X.; Wood, V.; Verevkin, A. A.; Ahn, C. H.; McKee, R. A.; Walker, F. J.; Specht, E. D. Epitaxial growth of $Pb(Zr_{0.2}Ti_{0.8})O_3$ on Si and its nanoscale piezoelectric properties. *Appl. Phys. Lett.* **2001**, *78*, 2034−2036.
(61) Suslick, K. S. Sonochemistry. *Science* **1990**, *247*, 1439−1445.
(62) Yusof, N. S. M.; Babgi, B.; Alghamdi, Y.; Aksu, M.; Madhavan, J.; Ashokkumara, M. Physical and chemical effects of acoustic cavitation in selected ultrasonic cleaning applications. *Ultrason. Sonochem.* **2016**, *29*, 568−576.
(63) Mason, T. J.; Peters, D.. *Practical Sonochemistry Power Ultrasound Uses and Applications, Woo electrostaticpotential on water/electrode systems dhead Publishing*; Woodhead Publishing, 2002.
(64) Siepmann, J. I.; Sprik, M. Influence of surface topology and. *J. Chem. Phys.* **1995**, *102*, 511−524.
(65) Harasima, A. *Molecular Theory of Surface Tension*; Wiley Blackwell, 2007, pp. 203237.
(66) Ball, P. Water-an enduring mystery. *Nature* **2008**, *452*, 291−292.
(67) Futera, Z.; English, N. J. Communication: Influence of external static and alternating electric fields on water from long-time non-equilibrium ab initio molecular dynamics. *J. Chem. Phys.* **2017**, *147*, 031102.
(68) Schindler, M.; Hawthornea, F. C.; Baur, W. H. Metastructures: Homeomorphisms between complex inorganic structures and three-dimensional nets. *Acta Crystallogr.* **1999**, *55* (6), 811−829.
(69) Occelli, M. L.; Schweizer, A. E.; Fild, C.; Schwering, G.; Eckert, H.; Auroux, A. Gallioaluminosilicate molecular sieves with the faujasite structure. *J. Catal.* **2000**, *192*, 119−127.
(70) Harrison, W. T. A.; Gier, T. E.; Moran, K. L.; Nicol, J. M.; Eckert, H.; Stucky, G. D. Structures and properties of new zeolite x-type zincophosphate and beryllophosphate molecular-sieves. *Chem. Mater.* **1991**, *3*, 27−29.
(71) Nenoff, T. M.; Harrison, W. T. A.; Gier, T. E.; Nicol, J. M.; Stucky, G. D. Structural characterization of a dehydrated magnesium sodium beryllophosphate faujasite phase. *Zeolites* **1992**, *12*, 770−775.
(72) Hu, X.; Bai, J.; Hong, H.; Chunping, L. Supercritical carbon dioxide anchored highly dispersed silver nanoparticles on 4A-zeolite and selective oxidation of styrene performance. *CrystEngcomm* **2016**, *18* (14), 2469−2476.
(73) Wang, Z.; Liu, Y.; Jiang, J.-G.; He, M.; Wu, P. Synthesis of ZSM-5 zeolite hollow spheres with a core/shell structure. *J. Mater. Chem.* **2010**, *20*, 10193−10199.
(74) Liu, S.; Cheng, Z.; Ying, L.; Sun, J.; Cai, K.; Huang, S.; Jing, L.; Wang, S.; Xinbin, M. Improved Catalytic Performance in Dimethyl Ether Carbonylation over Hierarchical Mordenite by Enhancing Mass Transfer. *Ind. Eng. Chem. Res.* **2020**, *59* (31), 13861−13869.

https://doi.org/10.1021/acsomega.4c04461
ACS Omega 2024, 9, 39673−39681